Edge Momentum Transport by Neutrals: an Interpretive Numerical Framework

J.T. Omotani[1], S.L. Newton[1,2], I. Pusztai[1], E. Viezzer[3,4], T. Fülöp[1] and the ASDEX Upgrade Team

[1]Department of Physics, Chalmers University of Technology, 41296 Gothenburg, Sweden
[2]CCFE, Culham Science Centre, Abingdon, Oxon, OX14 3DB, UK
[3]Max-Planck-Institute for Plasma Physics, Boltzmannstr. 2, 85748 Garching, Germany
[4]Department of Atomic, Molecular, and Nuclear Physics, University of Seville, Avda. Reina Mercedes, 41012 Seville, Spain

Corresponding Author: omotani@chalmers.se

Abstract:
Due to their high cross-field mobility, neutrals can contribute to momentum transport even at the low relative densities found inside the separatrix and they can generate intrinsic rotation. We use a charge-exchange dominated solution to the neutral kinetic equation, coupled to neoclassical ions, to evaluate the momentum transport due to neutrals. Numerical solutions to the drift-kinetic equation allow us to cover the full range of collisionality, including the intermediate levels typical of the tokamak edge. In the edge there are several processes likely to contribute to momentum transport in addition to neutrals. Therefore, we present here an interpretive framework that can evaluate the momentum transport through neutrals based on radial plasma profiles. We demonstrate its application by analysing the neutral angular momentum flux for an L-mode discharge in the ASDEX Upgrade tokamak. The magnitudes of the angular momentum fluxes we find here due to neutrals of 0.6 N m are comparable to the net torque on the plasma from neutral beam injection, indicating the importance of neutrals for rotation in the edge.

1 Introduction

Momentum transport in the tokamak edge is a crucial issue since rotation suppresses magnetohydrodynamic instabilities such as resistive wall modes [1–4] and flow shear in the edge suppresses turbulence, leading to high-confinement mode (H-mode) operation [5]. Neutral particles are always present in the edge of the confined plasma volume, and despite their low relative density can contribute strongly to transport in hydrogenic plasmas due to their high cross-field mobility, as has been demonstrated theoretically [6–15]. The influence of neutrals on confinement has also been observed experimentally [16–18] and the poloidal location of gas-fuelling, inboard versus outboard, has been seen to be important for the low- to high-confinement transition threshold [19–21].

It has been shown previously that when neutrals dominate the angular momentum transport, the radial electric field and hence toroidal rotation can be self-consistently calculated [13–15]. It was also shown that the neutrals can generate intrinsic rotation, since a toroidal heat flux in the ions drives a radial flux of angular momentum through neutrals, as explained in [14]. However, there will be other contributions, potentially of

similar or greater magnitude, for instance from turbulence, ion orbit losses [22, 23], non-axisymmetric magnetic fields [24] or finite orbit width effects [25]. It is therefore important to evaluate the momentum transport due to neutrals from experimental profiles, so that the magnitudes of the various effects can be compared. Analytical solutions [13, 14] rely on asymptotic ordering of the collisionality into the Pfirsch-Schlüter (high collisionality) or banana (low collisionality) regimes. However, the conditions typical in the edge plasma produce order unity collisionality, for example $\nu_{\mathrm{ii}} L_\parallel / v_T \sim 0.2-0.5$ for the profiles we show in Section 3, where v_T is the thermal velocity, ν_{ii} the ion-ion collision rate and $L_\parallel = \oint d\theta \left(dl_\parallel / d\theta \right) / 2\pi$ the parallel connection length. Recently, the radial electric field and toroidal rotation have been calculated numerically from the constraint that the angular momentum flux through neutrals vanishes in steady state in the absence of external torque [15] that is, as noted above, assuming that the neutrals dominate the momentum transport and also that the radial gradient of the neutrals is the dominant profile gradient. The latter assumption makes the calculation of the momentum flux local (otherwise it would depend on, for instance, the radial gradient of the toroidal rotation and hence on second derivatives of the density, temperature, etc.). Here, in order to avoid these assumptions, we introduce a new approach which takes the background plasma profiles, including the radial electric field, as given, allowing us to calculate the angular momentum flux through neutrals directly, without requiring that they are the only channel for momentum transport. We solve the drift-kinetic equation for ions numerically to remove the restriction to asymptotic collisionality regimes imposed by analytical solutions. This provides an interpretive tool that can be applied to experimental data in order to compare the magnitude of the neutral momentum transport to other mechanisms and to external sources of momentum such as neutral beam injection (NBI) heating. The interpretive approach is derived in Section 2 and applied to an L-mode discharge from ASDEX Upgrade (AUG) in Section 3. We discuss the implications of the results in Section 4.

2 Neutral momentum transport

We outline here the calculation of the angular momentum flux through hydrogenic[1] neutrals, which are coupled by charge-exchange (CX) to kinetic ions. Integrated over a flux surface, the radial flux of toroidal angular momentum carried by the neutral population is $V' \left\langle R\hat{\boldsymbol{\zeta}} \cdot \mathbf{\Pi}_{\mathrm{n}} \cdot \nabla\psi \right\rangle$ where $\mathbf{\Pi}_{\mathrm{n}} = m_{\mathrm{i}} \int d^3 v \, \boldsymbol{v}\boldsymbol{v} f_{\mathrm{n}}$ is the stress tensor of the neutrals, f_{n} is the distribution function of the neutrals, $2\pi\psi$ is the poloidal flux, V is the volume enclosed by a flux surface, a prime denotes a derivative with respect to ψ, R is the major radius, $\hat{\boldsymbol{\zeta}} = \nabla\zeta / |\nabla\zeta|$ with ζ the toroidal angle (increasing in the co-current direction), m_{i} is the mass of the ions or neutrals and $\langle ... \rangle$ is the flux surface average.

Our solution to the kinetic equation for f_{n} relies on several approximations. We take a short CX mean-free-path (MFP) expansion; although the MFP is not always short compared to profile length scales in the edge, it was found in [12] that the approximation is surprisingly accurate, compared to a full solution allowing arbitrary MFP for a special class of self-similar profiles. The short MFP approximation means that the neutrals are

---

[1]Hydrogenic plasmas are special since CX interactions preserve the number of neutrals. In a non-hydrogenic plasma, presuming that it is hot enough for multiply-charged ions to predominate, the CX reaction of a neutral will produce two ions, which will both be confined by the magnetic field until they are ionized, unless the neutral density is so high that they can rapidly undergo further CX reactions with neutrals. The chain of neutral flights between multiple CX interactions, which is the process underlying the large transport we describe in this paper, is thus absent in non-hydrogenic plasmas.

dominated by CX collisions with the ions, so we do not describe the effects of the population of cold neutrals that penetrate from the scrape-off layer without charge-exchanging and which produce a drag on the edge plasma. We neglect ionization, but this is most important for the determination of the neutral density profile, which we take as an input; ionization affects the momentum transport only by changing the effective collision rate [9]. We use a simplified CX collision operator [7] that allows us to close the neutral kinetic equation in an efficient way [9], as described below. These approximations allow us to avoid the computational expense of Monte Carlo neutral codes, e.g. EIRENE [26], while retaining coupling to the kinetic ion distribution, rather than only a drifting Maxwellian as implemented in [26].

The steady state neutral kinetic equation then takes the form [9]

$$\boldsymbol{v} \cdot \nabla f_{\mathrm{n}} = \frac{1}{\tau_{\mathrm{CX}}} \left(\frac{n_{\mathrm{n}}}{n_{\mathrm{i}}} f_{\mathrm{i}} - f_{\mathrm{n}} \right), \tag{1}$$

where n_{n} and n_{i} are the neutral and ion densities and f_{i} is the ion distribution function. $\tau_{\mathrm{CX}}^{-1} = n_{\mathrm{i}} \langle \sigma v \rangle_{\mathrm{CX}}$ is the characteristic rate for charge-exchange interactions with $\langle \sigma v \rangle_{\mathrm{CX}}$ the thermal charge exchange rate, where $\langle \sigma v \rangle_{\mathrm{CX}} = 4.21 \times 10^{-14} \mathrm{~m^3\,s^{-1}}$ for Deuterium ions and neutrals at 300 eV [27], which is a typical temperature value of the profiles we use in Section 3. Solving perturbatively for small $\tau_{\mathrm{CX}} v_T / L$, where v_T is the thermal speed and L is a characteristic length scale of the background profiles,

$$f_{\mathrm{n}}^{(0)} = \frac{n_{\mathrm{n}}}{n_{\mathrm{i}}} f_{\mathrm{i}}, \tag{2}$$

$$f_{\mathrm{n}}^{(1)} = -\tau_{\mathrm{CX}} \boldsymbol{v} \cdot \nabla \left(\frac{n_{\mathrm{n}}}{n_{\mathrm{i}}} f_{\mathrm{i}} \right). \tag{3}$$

$f_{\mathrm{n}}^{(0)}$ contributes a term to the angular momentum flux which, being proportional to $\boldsymbol{\Pi}_{\mathrm{i}}$, is $\mathcal{O}(\delta^2)$ in the gyroradius expansion [28] and therefore negligible, where $\delta = \rho / L$ and ρ is the gyroradius. Thus we need keep only $f_{\mathrm{n}}^{(1)}$, which gives a large contribution ($\mathcal{O}(\delta)$ in the gyroradius expansion) to the radial flux of angular momentum because it is strongly anisotropic in velocity perpendicular to the magnetic field. Hence the flux of angular momentum due to the neutrals, integrated over a flux surface, becomes

$$V' \left\langle R \hat{\boldsymbol{\zeta}} \cdot \boldsymbol{\Pi}_{\mathrm{n}} \cdot \nabla \psi \right\rangle = -m_{\mathrm{i}} \tau_{\mathrm{CX}} V' \left\langle R \int d^3 v \left(\hat{\boldsymbol{\zeta}} \cdot \boldsymbol{v} \right) (\nabla \psi \cdot \boldsymbol{v}) \boldsymbol{v} \cdot \nabla \left(\frac{n_{\mathrm{n}}}{n_{\mathrm{i}}} f_{\mathrm{i}} \right) \right\rangle$$

$$\approx -m_{\mathrm{i}} \tau_{\mathrm{CX}} \frac{d}{d\psi} \left(V' \left\langle \frac{R n_{\mathrm{n}}}{n_{\mathrm{i}}} \int d^3 v \left(\hat{\boldsymbol{\zeta}} \cdot \boldsymbol{v} \right) (\nabla \psi \cdot \boldsymbol{v})^2 f_{\mathrm{i}} \right\rangle \right), \tag{4}$$

neglecting $\nabla^2 \psi$ and using the identities $\langle \nabla \cdot \boldsymbol{A} \rangle = \frac{1}{V'} \frac{d}{d\psi} (V' \langle \nabla \psi \cdot \boldsymbol{A} \rangle)$ for any $\boldsymbol{A}$ [28] and $\boldsymbol{v v} : \nabla \left(R \hat{\boldsymbol{\zeta}} \right) = 0$[2]. Including the gyroradius correction, the ion distribution function at the particle position $\boldsymbol{r}$ is

$$f_{\mathrm{i}}(\boldsymbol{r}) = f_{\mathrm{i,gc0}}(\boldsymbol{r}) - \frac{e \Phi_1}{T_{\mathrm{i}}} f_{\mathrm{i,gc0}}(\boldsymbol{r}) - \boldsymbol{\rho} \cdot \nabla f_{\mathrm{i,gc0}}(\boldsymbol{r}) + g_{\mathrm{i}}(\boldsymbol{r}), \tag{5}$$

where $f_{\mathrm{i,gc0}}$ is a Maxwellian, $\boldsymbol{\rho} = \boldsymbol{r} - \boldsymbol{R}_{\mathrm{gc}}$ is the gyroradius vector with $\boldsymbol{R}_{\mathrm{gc}}$ the guiding centre position, $\Phi_1 = \Phi - \langle \Phi \rangle$ is the poloidally varying part of the electrostatic potential

---

[2]This identity follows from the fact that $\boldsymbol{v v}$ is a symmetric tensor, while $\nabla \left(R \hat{\boldsymbol{\zeta}} \right)$ is antisymmetric.
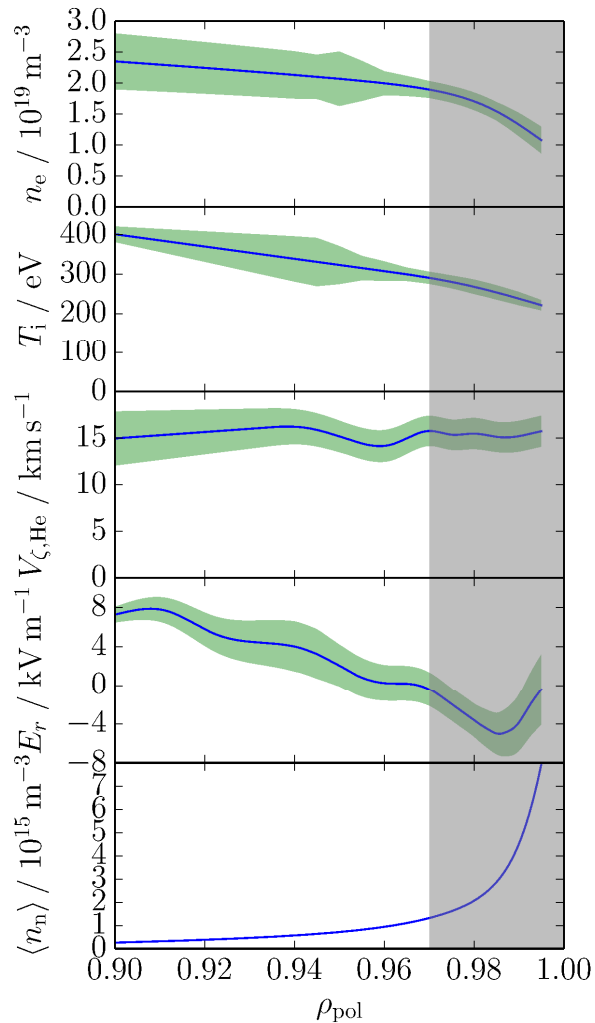
FIG. 1: *Profiles from AUG discharge #26601 as a function of ρ_{pol}. From the top: electron density n_{e}; ion temperature T_{i}; toroidal velocity of helium impurity $V_{\zeta,\mathrm{He}}$; and radial electric field E_r at the outboard midplane. Experimental uncertainties are indicated by the green shaded regions. At the bottom is the input profile we use for the flux surface average of the neutral density $\langle n_{\mathrm{n}} \rangle$, from a KN1D simulation. Grey shaded area is within a drift orbit width of the separatrix.*

Φ and 0, 1 subscripts refer to the order in δ. The first two terms do not contribute to (4) as they are isotropic in $\boldsymbol{v}$. We obtain the non-adiabatic piece of the perturbed distribution function, $g_{\mathrm{i}} = f_{\mathrm{i},gc1} + e_{\mathrm{i}}\Phi_1 f_{\mathrm{i},gc0}/T_{\mathrm{i}}$ from numerical solutions of the first order drift kinetic equation using the PERFECT neoclassical solver (run here in radially-local mode) [29], which assume that the flow is subsonic, $\boldsymbol{V} \sim \mathcal{O}(\delta v_T)$.

As noted in the introduction, this system was used to explore the effects of magnetic geometry and collisionality on intrinsic rotation driven by momentum transport through neutrals [15, 30]. In the next section we introduce the interpretive framework which can be used to diagnose experimental results.

3   Interpretive modelling of momentum flux

We have evaluated the angular momentum flux through neutrals for L-mode profiles from the AUG discharge #26601, shown in FIG. 1, in order to demonstrate the potential of our interpretive tool. This takes profiles of ion density n_i and temperature T_i, radial electric field E_r and neutral density n_n as inputs, as well as the magnetic equilibrium, to calculate the angular momentum flux as described in the previous section. It would also be possible to constrain the neoclassical solutions with the toroidal rotation profile of any ion species instead of E_r.

For the AUG case, CXRS measurements were performed on the He^{2+} impurity to measure the ion temperature (assumed equal to the He^{2+} temperature) and both toroidal and poloidal He^{2+} rotation velocity measurements were used to infer E_r [31], which is the same for all species. (Note that this avoids any ambiguity involved in relating main ion to impurity rotation.) Electron density was measured with the Thomson scattering, Lithium beam and interferometry diagnostics; we neglect the impurity density, taking $n_i = n_e$. Profiles are plotted as functions of the normalized flux label $\rho_{pol} = \sqrt{\psi/\psi_{sep}}$ where ψ_{sep} is the value of ψ at the separatrix and we take $\psi = 0$ at the magnetic axis. We consider the region $0.90 < \rho_{pol} < 1.00$, where the E_r measurements are available.

To obtain neutral density profiles, we ran KN1D [32] using plasma profiles at the outboard midplane, except in FIG. 4 at the end of this section where we take into account the different radial profiles of neutral density at different poloidal positions. We extend the profiles into the scrape-off layer as exponentials, with decay lengths of 3 cm for the density and 0.5 cm for the electron and ion temperatures. KN1D's molecular pressure input was chosen to give a value of $n_n \approx 10^{16}$ m^{-3} at the separatrix, consistent with the low-field side neutral density modelled in [33]. We use the output of KN1D to set the flux surface average of the neutral density $\langle n_n \rangle$, which we keep fixed while exploring the effect of different poloidal profiles. FIG. 2 compares the effect on the angular momentum carried by the neutrals of different poloidal widths of the neutral density profile: poloidally uniform; localized as a Gaussian around the outboard midplane $\theta = 0$, $n_n \propto \exp(-\theta^2/2w_\theta^2)$ with $w_\theta = \pi/5$; and localized as a δ-function at the outboard midplane $n_n \propto \delta(\theta)$. FIG. 3 compares the effect of different poloidal locations of Gaussian-localized neutral density profiles, $n_n \propto \exp(-(\theta - \theta_0)^2/2w_\theta^2)$ with $w_\theta = \pi/5$ again for three values of the central position θ_0: outboard midplane $\theta_0 = 0$; inboard midplane $\theta_0 = \pi$; and the closest position to the X-point $\theta_0 \approx 4.49$.

Near the separatrix the scale lengths of the density $L_n = (d \ln n_i/dr)^{-1}$ and temperature $L_T = (d \ln T_i/dr)^{-1}$ become relatively short, significantly less than the MFP for CX. In addition, the contribution of cold neutrals that penetrate from the scrape-off layer without charge-exchanging, and which we do not treat, is most important close to the separatrix. We therefore exclude the region outside $\rho_{pol} = 0.97$, indicated by the shaded area in FIG. 1, in the presentation of our results.

We discuss first the magnitude of the flux, using the case of poloidally uniform neutrals for illustration. We will then consider the effect of poloidal variation, but note that the poloidally varying profiles are artificial in the sense that they fall to zero rather than a finite background value away from the peak. For poloidally uniform neutrals, the outward flux of co-current toroidal angular momentum passing through a flux surface reaches -0.6 N m, as shown in FIG. 2. The discharge had 1.1 MW of NBI heating with 39.8 keV particles; the momentum is deposited at a tangency radius $R_{NBI} = 0.93$ m and so the external momentum input from the NBI is 1.05 N m (indicated as the dashed horizontal
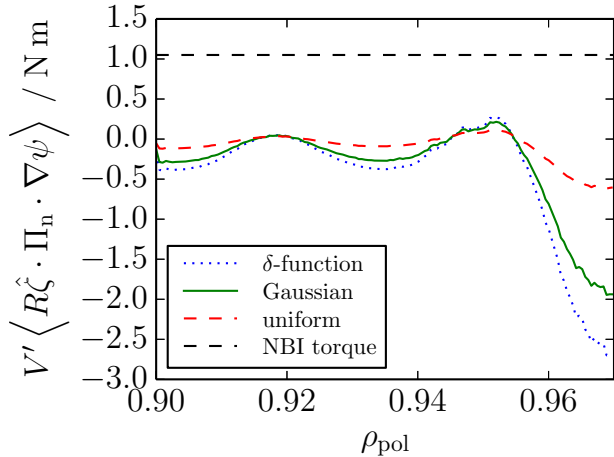
FIG. 2: *Comparison of outward flux of toroidal angular momentum through neutrals, integrated over the flux surface at $\rho_{\rm pol}$, for different poloidal profile shapes: δ-function at outboard midplane (blue, dotted), Gaussian with width $\pi/5$ rad centred at outboard midplane (green, solid) and uniform (red, dashed). The total angular momentum flux from the NBI source is indicated as the horizontal, dashed line. Positive values represent radially outward flux of co-current angular momentum.*

line in FIG. 2), of a similar magnitude to the total (surface-integrated) momentum flux carried by the neutrals. The NBI input gives the net outward flux of angular momentum carried by all mechanisms through our simulation domain in the plasma edge region, assuming that the NBI momentum is predominantly deposited in the core plasma and provides the only source of angular momentum. The neutrals thus carry a significant angular momentum flux near the plasma edge and can be expected to play an important role in regulating the plasma rotation in L-mode. The momentum flux fluctuates radially, as well as generally decreasing in magnitude away from the separatrix. These fluctuations are caused by the fluctuations in the gradient of the experimental radial electric field profile. However, these fluctuations could be eliminated by variations in the electric field profile within the experimental uncertainties, as shown in Appendix A.

For comparison one can make a simple estimate of the expected angular momentum flux through the neutrals. Assume that the fast neutrals, those coming from a charge exchange reaction with a hot ion in the confined plasma, escape immediately from the confined region. Then the total momentum carried out of the plasma is $\Gamma_{\rm n} m_{\rm i} \bar{V}_\zeta R_{\rm out} \approx$ 0.3 N m where $\Gamma_{\rm n} \approx 2 \times 10^{21}$ s^{-1} is the total inward flux of neutrals (estimated from the flux density across the separatrix of 10^{20} m^{-2} s^{-1} simulated by KN1D), $\bar{V}_\zeta \approx 20$ km s^{-1} is a typical toroidal rotation velocity and $R_{\rm out} \approx 2$ m is a typical radius in the outboard edge region of the plasma. This estimate is similar in magnitude to our prediction but has the opposite sign; this is a consequence of the very different assumptions made. For this estimate each neutral experiences only one CX interaction and acts purely as a momentum sink. On the other hand in the short MFP model we use, each neutral undergoes several CX interactions. The direction of the flux (inward or outward) is then influenced by the directions of the gradients in both neutral density and plasma toroidal rotation, heat flux, etc. because neutrals exchange momentum between different flux surfaces. In particular there can be an inward pinch of momentum due to the density gradient of the neutrals. On a given flux surface there are more neutrals coming from the outside than the inside, all carrying the momentum picked up from a CX reaction with an ion. Note that, as we
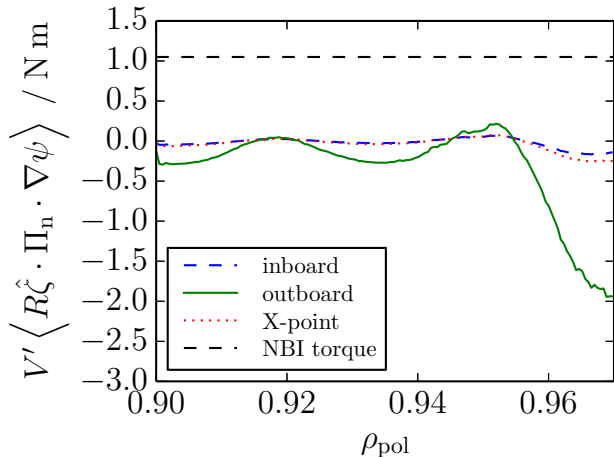
FIG. 3: Comparison of outward flux of toroidal angular momentum through neutrals, integrated over the flux surface at $\rho_{\rm pol}$, for different poloidal positions of the neutral density peak: inboard midplane (blue, dashed), outboard midplane (green, solid) and the nearest poloidal position to the X-point (red, dotted). Poloidal profile of the neutrals is Gaussian with width $\pi/5$ rad. The total angular momentum flux from the NBI source is indicated as the horizontal, dashed line. Positive values represent radially outward flux of co-current angular momentum.

see in FIG. 1, the toroidal rotation does not change much across our domain; thus the momentum carried by each inward or outward going particle will be similar, so that this effect gives rise to an inward flux of angular momentum.

Poloidal localization of the neutrals can enhance the angular momentum flux. In FIG. 2 we compare the momentum flux for three different assumed poloidal profiles: uniform, Gaussian (with standard deviation $\pi/5$ rad) or δ-function. The localized profiles are centred at the outboard midplane. For ease of comparison we have used the same flux-surface averaged neutral density profile for all of the curves. In reality, the neutral distribution will be some combination of a roughly uniform piece from wall recycling and a localized part near the gas fuelling valve (represented by the Gaussian shape here), so the enhancement above the uniform level due to outboard localization could be expected to be more moderate than the limiting case shown. Previous work, both analytical [13, 14] and numerical [15], used δ-function localized neutrals for convenience. We can see from FIG. 2 that there is not a major difference between this approximation and the case of neutrals localized as a Gaussian, with both the trends and order of magnitude being correctly captured, although the sharper localization of the δ-function does further enhance the momentum flux.

The neutrals provide more effective transport of toroidal angular momentum when they are on the outboard side of the tokamak than on the inboard side or near the X-point, due to the larger major radius and poloidal magnetic field $B_{\rm p}$, as can be seen from (4), noting that $|\nabla\psi| = RB_{\rm p}$. This is demonstrated by FIG. 3 which compares the momentum flux through Gaussian localized neutrals centred at the outboard midplane, inboard midplane and adjacent to the X-point where we have used the same $n_{\rm n}(\psi)$ calculated at the outboard midplane, highlighting the importance of the poloidal location of the neutrals for the angular momentum flux that they carry. However due to flux expansion the neutral density decays more rapidly as a function of ψ if the fuelling location is at the inboard midplane or X-point. KN1D allows rapid calculation of the radial profiles of
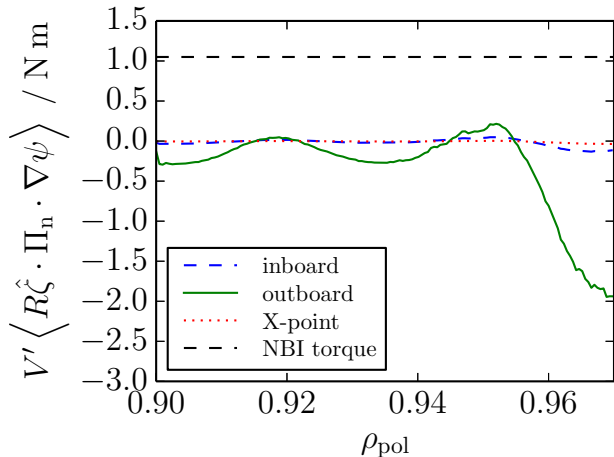
FIG. 4: *Same as FIG. 3 but using radial profiles $n_n(\psi)$ calculated at the same poloidal position as the neutral density peak.*

neutral density at each poloidal location using the plasma profiles as a function of minor radius. The angular momentum flux is then further suppressed, as can be seen in FIG. 4. This demonstrates the need to reconstruct the density profile of neutrals accurately when trying to understand their effect on toroidal rotation and momentum transport.

4 Discussion

We have demonstrated here that charge-exchanging neutrals can carry a significant angular momentum flux in the tokamak edge. The formalism developed in [13, 14] and first implemented numerically in [15] has been extended, to enable interpretive studies evaluating the momentum transport through neutrals for experimental profiles and equilibria. In this interpretive mode, the radial variation of the background profiles does not have to be neglected compared to the radial gradient of the neutral density. We model an L-mode discharge from AUG to demonstrate this capability and show that a significant flux of angular momentum, comparable in magnitude to the total momentum input from NBI, can be carried by the neutrals, motivating further application to experimental data in future.

The approach taken here allows rapid experimentation with parameters and profiles and provides both qualitative insight and at least order of magnitude estimates of the momentum transport due to neutrals. Despite the limitations of the modelling described here, some conclusions are clear. The strength of the neutral momentum transport is much larger for neutrals located on the outboard side of the tokamak than on the inboard side. This is due both to the smaller moment of force at smaller major radius and to the smaller physical-space gradients of flux-function plasma profiles which have poloidally constant gradients in ψ-space, as $|\nabla\psi| = RB_p$ is smaller on the inboard side. Likewise near the X-point, where B_p is small, the influence of the neutrals will be weak. Thus the influence of neutrals on the plasma rotation may be minimized by fuelling from the inboard side or X-point. On the other hand, if it is desired to drive intrinsic rotation using the neutral angular momentum flux [13–15], then this will compete more effectively with other momentum transport channels if the neutrals are located on the outboard side and may be able to generate substantial radial electric fields in H-mode pedestals.

Intrinsic rotation is particularly important for future tokamaks such as ITER since

the angular momentum source from NBI heating will be weaker in larger devices. It should be noted that in ITER, neutral penetration inside the separatrix is expected to be small compared to current devices and the fuelling scheme in ITER will be different from existing machines, with core fuelling being dominated by pellet injection rather than the gas puffing that we have considered here. A more complete study is of interest as momentum transport is the channel most sensitive to the presence of neutrals [9], for which neutrals may maintain an influence at the lowest relative densities. The interesting case is that with steep temperature profiles in H-mode and although our modelling is restricted to L-mode plasmas, it is in the region where the edge transport barrier will form in H-mode that neutrals are most important. However, modelling steep temperature gradients is extremely challenging since the deviation of the bulk ion distribution from a Maxwellian distribution is not small, so that a non-linear collision operator is needed, and the steep gradients also necessitate radially-global solutions. State of the art numerical solutions of the neutral kinetic equation couple only to a drifting-Maxwellian plasma [26]. However, the temperature gradient driven departure of the ions from a local Maxwellian distribution drives an angular momentum flux in the neutral distribution function [7, 14]. Thus when the external torque is large, so that the rotation-driven momentum flux dominates, the drifting-Maxwellian description of the bulk plasma is sufficient, but when there are steep temperature gradients, or for intrinsic rotation where the external torque vanishes, a kinetic model for the plasma is needed. In the linear region we have considered, where standard neoclassical theory and modelling are valid, the transport is proportional to the gradients, so significantly stronger momentum transport through neutrals may be expected to arise in steep gradient regions, such as the H-mode pedestal. Quantitative evaluation, requiring the development of more sophisticated codes coupling fully kinetic neutrals to kinetic ions, remains a challenging subject for future research, which can build on existing progress in neoclassical pedestal modelling [29, 34–36].

Acknowledgements

A   Sensitivity to E_r

To demonstrate that the fluctuations of the angular momentum flux in FIG. 2 are due to the changing gradient of E_r, we have repeated the simulations taking for input a linear fit to E_r, shown in FIG. 5. FIG. 6 shows that indeed this linear E_r eliminates the fluctuations. The slight increase in magnitude of the angular momentum flux from about $\rho_{\mathrm{pol}} = 0.94$ to $\rho_{\mathrm{pol}} = 0.90$ is due to the increasing drive from the $E \times B$ rotation due to larger E_r, which compensates the decaying neutral density. The neutral density decreases by a factor of only ~ 2.4 from $\rho_{\mathrm{pol}} = 0.94$ to $\rho_{\mathrm{pol}} = 0.90$.
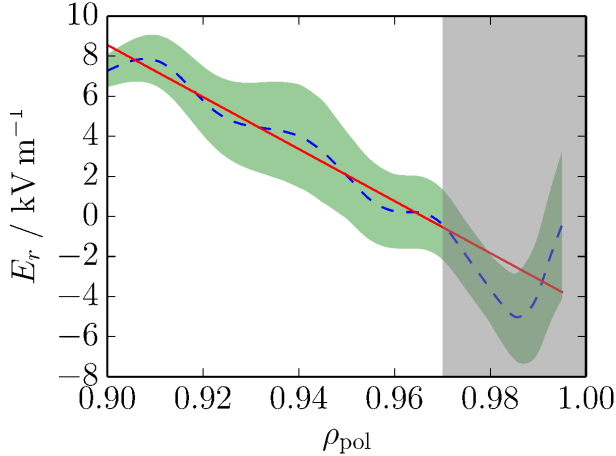
FIG. 5: *Least squares linear fit (red solid line) to E_r (blue dashed line) in the simulation domain $0.90 < \rho_{\mathrm{pol}} < 0.96$. Experimental uncertainties on E_r shown as green region.*

References

[1] BONDESON, A. et al., Phys. Rev. Lett. **72** (1994) 2709.

[2] STRAIT, E. J. et al., Phys. Rev. Lett. **74** (1995) 2483.

[3] GAROFALO, A. M. et al., Phys. Rev. Lett. **82** (1999) 3811.

[4] HENDER, T. et al., Nucl. Fusion **47** (2007) S128.

[5] TERRY, P. W., Rev. Mod. Phys. **72** (2000) 109.

[6] HAZELTINE, R. et al., Nucl. Fusion **32** (1992) 3.

[7] CATTO, P. J., Phys. Plasmas **1** (1994) 1936.

[8] HELANDER, P. et al., Phys. Plasmas **1** (1994) 3174.

[9] CATTO, P. J. et al., Phys. Plasmas **5** (1998) 3961.

[10] FÜLÖP, T. et al., Phys. Plasmas **5** (1998) 3398.

[11] FÜLÖP, T. et al., Phys. Plasmas **5** (1998) 3969.

[12] FÜLÖP, T. et al., Phys. Plasmas **8** (2001) 5214.

[13] FÜLÖP, T. et al., Phys. Rev. Lett. **89** (2002) 225003.

[14] HELANDER, P. et al., Phys. Plasmas **10** (2003) 4396.

[15] OMOTANI, J. et al., Nuclear Fusion **56** (2016) 124002.

[16] VERSLOOT, T. W. et al., Plasma Phys. Controlled Fusion **53** (2011) 065017.

[17] JOFFRIN, E. et al., "Impact of divertor geometry on ITER scenarios performance in the JET metallic wall", [EX/P5-40] paper presented at 25th IAEA Int. Conf. on Fusion Energy St Petersburg 2014.
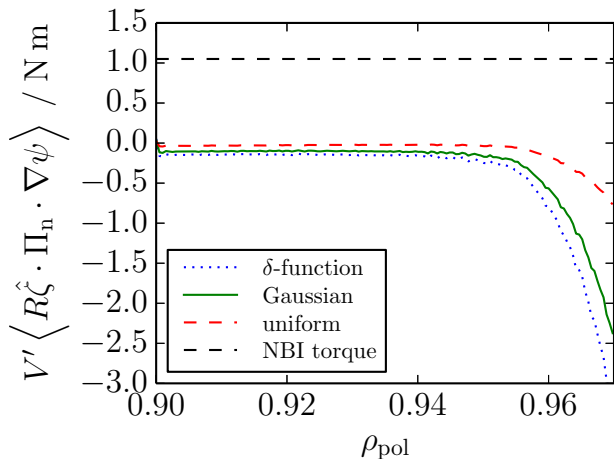
FIG. 6: Using linear fit for E_r shown in FIG. 5 as input for simulations, comparison of outward flux of toroidal angular momentum through neutrals, integrated over the flux surface at $\rho_{\rm pol}$, for different poloidal profile shapes: δ-function at outboard midplane (blue, dotted), Gaussian with width $\pi/5$ rad centred at outboard midplane (green, solid) and uniform (red, dashed). The total angular momentum flux from the NBI source is indicated as the horizontal, dashed line. Positive values represent radially outward flux of co-current angular momentum.

[18] TAMAIN, P. et al., J. Nucl. Mater. **463** (2015) 450.

[19] FUKUDA, T. et al., Plasma Phys. Controlled Fusion **42** (2000) A289.

[20] VALOVIC, M. et al., Plasma Phys. Controlled Fusion **44** (2002) A175.

[21] FIELD, A. R. et al., Plasma Phys. Controlled Fusion **46** (2004) 981.

[22] SHAING, K. C. et al., Phys. Rev. Lett. **63** (1989) 2369.

[23] STOLTZFUS-DUECK, T., Phys. Plasmas **19** (2012).

[24] NAVE, M. F. F. et al., Phys. Rev. Lett. **105** (2010) 105005.

[25] PUSZTAI, I. et al., Plasma Phys. Control. Fusion **58** (2016) 085001.

[26] REITER, D. et al., Fusion Sci. Technol. **47** (2005) 172.

[27] SUMMERS, H. P., *The ADAS User Manual, v. 2.6*, http://www.adas.ac.uk, 2004.

[28] HELANDER, P. et al., *Collisional transport in magnetized plasmas*, Cambridge University Press, 2002.

[29] LANDREMAN, M. et al., Plasma Phys. Controlled Fusion **56** (2014) 045005.

[30] OMOTANI, J. T. et al., J. Phys. Conf. Ser. (2016) in press.

[31] VIEZZER, E. et al., Nucl. Fusion **53** (2013) 053005.

[32] LABOMBARD, B., *KN1D: A 1-D space, 2-D velocity, kinetic transport algorithm for atomic and molecular hydrogen in an ionizing plasma*, Plasma Science and Fusion Center, Massachusetts Institute of Technology, 2001.

[33] VIEZZER, E. et al., Plasma Physics and Controlled Fusion **53** (2011) 035002.

[34] CATTO, P. J. et al., Plasma Phys. Control. Fusion **55** (2013) 045009.

[35] BATTAGLIA, D. J. et al., Phys. Plasmas **21** (2014) 072508.

[36] DORF, M. A. et al., Phys. Plasmas **23** (2016) 056102.